# CONTROLLABLE REFLECTION AND ABSORPTION IN THE MID-INFRARED WITH METAL-DIELECTRIC MICROSTRIP NANOANTENNAS

Alexandra Grigore[1], Ana Bărar[2], Doina Mănăilă-Maximean[3]

*We report theoretical assessments on a metal-dielectric metasurface-based nanoantenna operating in the 7-10 THz range. The metasurface is highly-responsive to the external electromagnetic field and exhibits a high dynamic range for reflection and absorption. The metasurface is addressable by means of input polarization, and can be used in a series of terahertz applications, from dichroic filters to tunable switches and absorbers.*

**Keywords:** Terahertz absorbers, frequency-selective surfaces, metasurfaces, metamaterials.

## 1. Introduction

The control of the electromagnetic field has been a keen interest in integrated radio-frequency, terahertz and optics research fields throughout their existence. Some electromagnetic field properties like negative reflection and refraction [1, 2], optical cloaking [3] and broadband nonlinearity [4], however, remained out of the scope of conventional paradigm, due to the limitation in material properties. Although predicted possible in theory [5], these limitations were experimentally lifted only twenty years ago, by exploiting collective oscillations in specially-developed artificial materials [6]. Due to the fact that the resonant response is dependent rather on the macroscopic configuration of the geometric shapes, sizes and relative placement than the individual atomic scattering properties of the composing materials, the structures are known as metamaterials if they are three-dimensional, or metasurfaces if they are two-dimensional [7]. Also, the electric and magnetic properties of the components play a role in establishing a response, which cannot be described by effective-medium approaches, like those used in host-guest systems [8, 9, 10]. In the case of metasurfaces, to achieve the same response over an extended surface, the unit configuration is repeated across $Ox$ and $Oy$, with the input field propagating on $Oz$. Taking a central wavelength $\lambda_0$ for the electromagnetic field, the sizes of the unit metasurface cell elements (rod lengths, thicknesses, radii) have to be in the $\lambda_0/10$ to $\lambda_0/5$ interval, while the overall cell size can be as large as $\lambda_0/2$. For higher sizes, the structure becomes to exhibit diffractive behavior, and the periodicity of the unit cell becomes predominant over the response of the cell elements [11]. Initially, metasurface configurations working

[1]Student, Faculty of Mechanics and Mechatronics, University POLITEHNICA of Bucharest, Bucharest, Romania
[2]Lecturer, Faculty of Electronics, Telecommunications and Information Technology, University POLITEHNICA of Bucharest, Romania
[3]Professor, Faculty of Applied Sciences, University POLITEHNICA of Bucharest, Romania, Corresponding Author, email: doina.manaila@upb.ro

in the GHz band used metal elements deposited on dielectric substrates [12, 13], but as miniaturization processes reduced the sizes of the cell elements so as to function in the THz and optical bands, hybrid [14, 15], and all-dielectric [14] configurations were used. The input optical field can also be prepared before interaction with the metasurface so as to exhibit a certain phase and polarization, by layering externally-addressable polymer-dispersed liquid crystals on top of the metasurface [16, 17]. In other cases, polymeric metasurfaces based on polyvinylidene have been shown to exhibit significant piezoelectric responses, which offer direct addressability through external electric fields [18]. All these enhancements extend the range of applications resulting from the control of the electromagnetic field properties, such as polarization control [19], electromagnetic cloaks [20], perfect lenses [21], electromagnetic sensors [22] and nonlinear harmonics enhancers [23] to name a few.

In this paper, we report studies on the electromagnetic field control capabilities of a metal-dielectric metasurface in the 7-10 THz spectral window, highlighting its enhanced capabilities to control the Fresnel coefficients and the associated phases. The metasurface exhibits a high dynamic range in the desired window, as well as dynamic sensitivity to the variation of both construction parameters and field properties. Due to these properties, our metasurface is a viable candidate for devices like controllable switches and field absorbers, field controllers and tunable dichroic filters.

## 2. **Architecture and simulation conditions**

We performed simulations in COMSOL Multiphysics - RF Module, which is a state-of-the art commercial application. The radio frequency module implements the homogeneous Helmholtz equation for the electric field:

$$\nabla \times \mu_r^{-1} (\nabla \times \mathbf{E}) - k_0^2 \left( \varepsilon_r - \frac{j\sigma}{\omega \varepsilon_0} \right) \mathbf{E} = 0 \tag{1}$$

on the specifically-designed metasurface architecture. In the above relation, $\mu_r$ is the relative magnetic permeability, $k_0$ is the vacuum wave number, $\varepsilon_r$ is the relative electric permittivity, $\sigma$ is the electric conductivity, $\omega$ is the angular frequency, $\varepsilon_0$ is the vacuum electric permittivity, $j^2 = -1$ is the complex imaginary number basis, and the 'del' operator is defined as $\nabla = \frac{\partial}{\partial x} + \frac{\partial}{\partial y} + \frac{\partial}{\partial z}$. By applying this equation on the spatial profile of the architecture we obtained the specific solutions of the electric field modes, as well as the reflection and absorption coefficients of the interface.

The spatial profile of the metasurface unit cell consists of a square air box with size $a = 36\mu m$, $z_b = 20\mu m$. On the $z = 0$ plane we have placed the polyamide substrate having thickness $h_{sb} = 8\mu m$, on top of which the plasmonic resonant structure was deposited. The structure follows a modified "T" shape, constructed by reuniting two rectangular rods. One rod has its long axis parallel to $Ox$, a length $l_1 = 12\mu m$, and width $w_1 = 1.2\mu m$. The other rod has its axis parallel to $Oy$, a length $l_2 = 12\mu m$ and width $w_2 = 3.6\mu m$. All components have the same height $h_m = 200nm$, and their relative positions are taken so that the "T" shape is centered on the substrate. The height of the polyamide substrate is $h_{sb} = 100\mu m$. The back of the polyamide substrate is fitted with a metallic

backplate oh thickness $h_b = 1\mu m$, in order to ensure no transmission. The sketch of the architecture is presented in Figure 1.

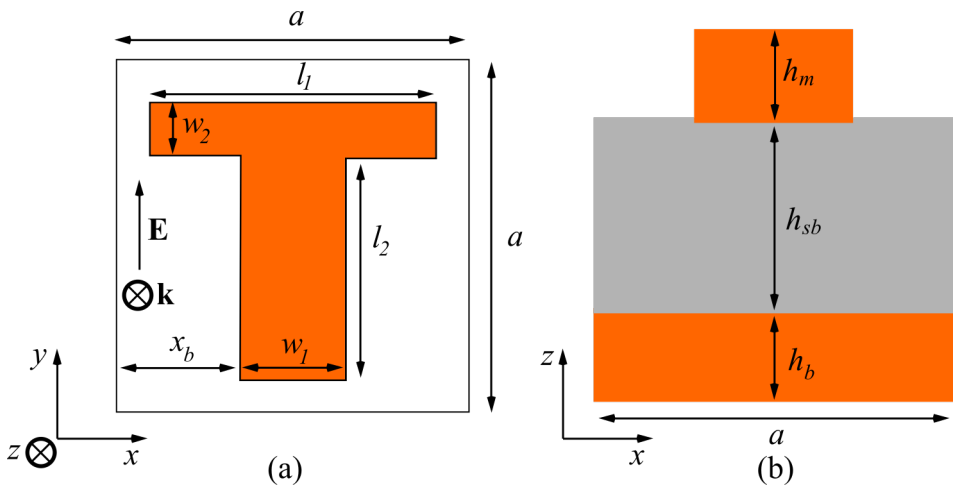


FIGURE 1. Reference configuration of the metacell, detailing the dimensional parameters: (a) Top view, and (b) side view.

In terms of material properties, the polyamide substrate used in our simulations is non-magnetic, (i.e., $\mu_r = 1$), has a relative electric permittivity $\varepsilon_r = 2.88 - j \cdot 0.09$ and a bulk electric conductivity $\sigma_{ply} = 6.6 \cdot 10^{-16} S/m$. The rods are made of gold, having $\varepsilon_r = 1$, $\mu_r = 1$ and $\sigma_{Au} = 4.09 \cdot 10^7 S/m$. Regarding simulations, the electromagnetic wave equation was applied to the air box and the architecture respecting the following boundary conditions: The electromagnetic field was set to propagate in the $Oz$ direction, at normal incidence on the metasurface, coming from an input port on the upper side of the air box. The electric field polarization is parallel to $Oy$, and the input power is $P_0 = 1pW$, in order to obtain watt-level intensities on the architecture element. The air box walls having their direction vector parallel to $Oy$ are fitted with a perfect electric conduction boundary condition, while the walls having their direction vector parallel to $Ox$ are fitted with a perfect magnetic conduction boundary condition. The two conditions are implemented to simulate a large-area periodic metasurface, not just the meta-cell. The thickness of the interface was simulated via a transition boundary condition having the penetration depth equal to the substrate thickness $h_{sb}$. The backplate of the substrate was covered with the conducting material under test (either gold or silver), to ensure that there is no transmission on the other side of the metasurface. To implement the discretized variant of the Helmholtz equation, a mesh with triangle sizes ranging from $\lambda_0/20$ to $\lambda_0/10$ was used, where $\lambda_0$ is the wavlength associated to the frequency in the center of the spectral window. The solver was set to find approximate solutions of the equation with a maximum tolerance of $10^{-3}$. Using this reference configuration, for gold and silver rods, we performed sweep measurements in which we changed either a geometric size or the input linear polarization of the field, and

we have evaluated the results. The parameters under evaluation were the reflection $(R)$ and absorption $(A)$ coefficients, which are linked by the relation $A = 1 - R$ due to the fact that the impedance boundary superimposed on the backplate of the substrate.

## 3. **Results and discussions**

The first assessment of the metasurface cell was the simulation of the spectral response as a function of the relative coordinate between the two rods. In the reference configuration, the base rod is placed on the median axis of the top rod, which corresponds to a relative coordinate $x_b = 7.15\mu m$ with respect to the corner of the metasurface cell. This parameter was varied between specific values $x_b = 4\mu m$ and $x_b = 10\mu m$. The results are shown in Figure 2.

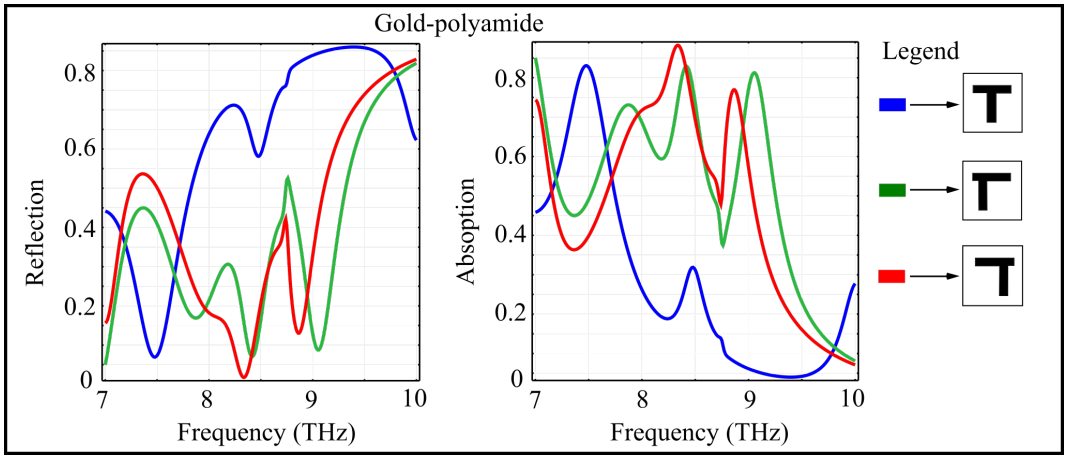


FIGURE 2. Spectral reflection and absorption of the gold-polyamide metasurface configuration, under variation of the relative coordinates of the base rod with respect to the top rod (configuration shown in the Legend inset).

In the symmetric "T"-shape configuration (blue line), the reflection of the metasurface varies between 0.1 and 0.9, with no sharp peaks, implying there are no parasitic oscillation modes on the interface. The reflection shows a pronounced dip at 7.45 THz, doubled by another, more shallow dip at 8.5 THz. In the asymmetric configuration with $x_b = 4\mu m$ (green line), the reflection peaks are attenuated between 0.1 and 0.4 for frequencies between 7 THz and 9.2 THz, with dips in the response at 8.45 THz and 9.2 THz. In the case of the configuration with $x_b = 10\mu m$ (red line), the reflection peaks suffer a shift towards lower frequencies, as well as a zero-reflection peak at $8.4THz$, corresponding to perfect absorption. As a general behavior, the absorption coefficient follows the model relation described in the previous section, with peaks being obtained exactly where the dips in reflection are located.

Another investigation was the evaluation of the spectral response as a function of the thickness of the top rod $w_1$ between fixed values of 0.8, 1.2 and 1.6 $\mu m$, and the rest of the parameters are those of the reference configuration. The results are presented in Figure 3.

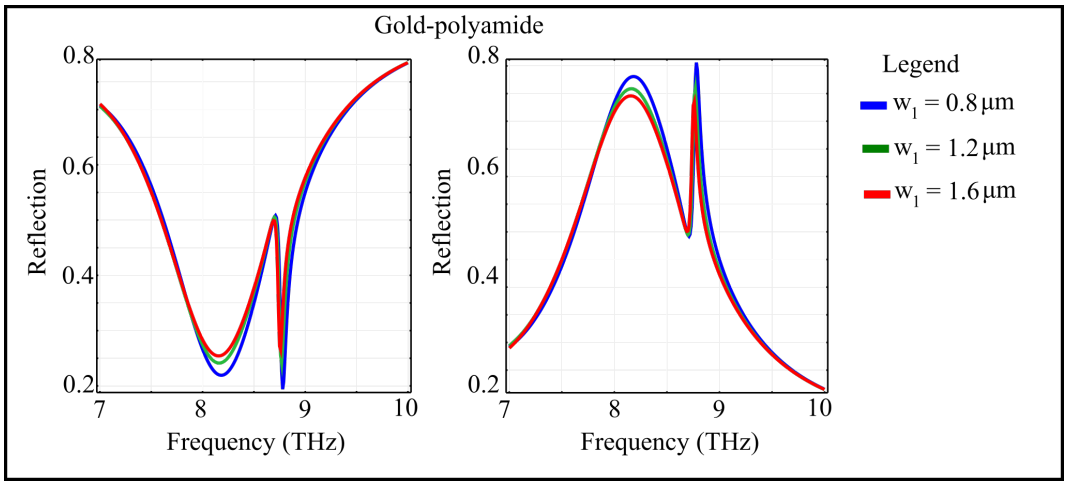


FIGURE 3. Spectral reflection and absorption of the gold-polyamide metasurface configuration, under variation of the thickness of the top rod $w_1$.

It can be seen that for all values of $w_1$, the reflection and absorption curves follow the same monotony, with relative shifts of the peaks and dips towards lower frequencies as the values of $w_1$ increase. The reflection curves exhibit two dips, one smooth, at 8.2 THz, and a relatively-sharp dip, at 8.76 THz, where the reflection drops to 0.19. The sharp dip also indicates the presence of a strong plasmonic oscillation between the two rods. Between these dips, the response shows a frequency-invariant reflection peak of 0.5, at 8.67 THz. This insensitivity is replicated in the 7−7.8 THz and 9.5−10 THz bands.

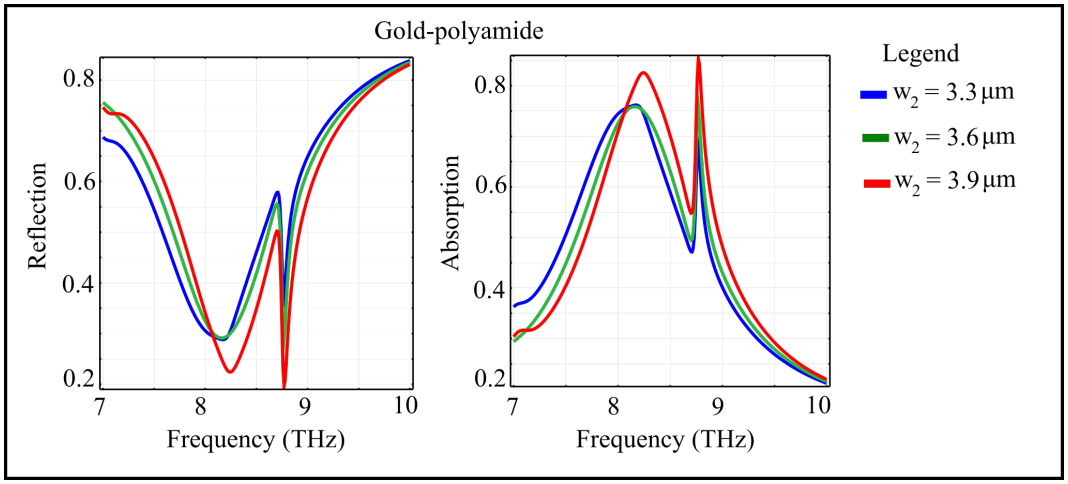


FIGURE 4. Spectral reflection and absorption of the gold-polyamide metasurface configuration under variataion of the thickness of the base rod $w_2$.

Another investigation that was performed was the assessment of the spectral response under the variation of the thickness of the base rod $w_2$ between fixed values of 3.3, 3.6 and 3.9 $\mu m$. The

results are shown in Figure 4. When varying $w_2$, the spectral dips in the reflection curves are shifted towards higher frequencies, from 8.76 THz in the reference configuration to 8.78 THz and 8.8 THz for $w_2 = 3.6\ \mu m$ and $w_2 = 3.9\ \mu m$ respectively. In the case of $w_2 = 3.9\ \mu m$, the reflection curve exhibits more accentuated dips, achieving values of 0.22 at 8.34 THz and 0.19 at 8.8 THz. The variation of $w_2$ also induces baseline variations in the reflection coefficient in the $7-8$ THz and $9-10$ THz bands, with a relative variation of approximately 0.05-0.1 and 0.03-0.05 respectively, when compared to the reference configuration.

Lastly, we have performed an investigation where the input field state of polarization was cycled through fixed values $\alpha = 0^\circ$ , $45^\circ$ and $90^\circ$ with respect to the reference configuration in which the electric field is parallel to the $Oy$ axis. The results are shown in Figure 5.

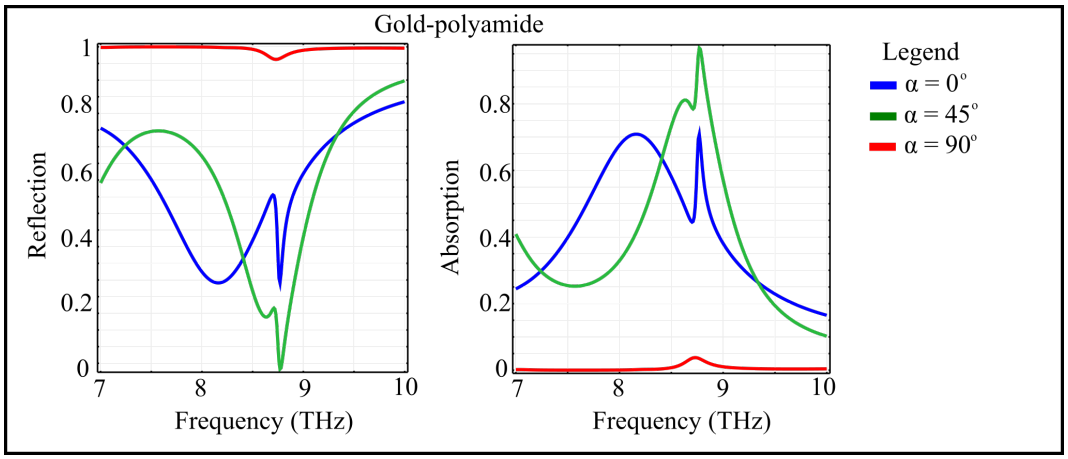


FIGURE 5. Spectral reflection and absorption of the gold-polyamide metasurface configuration under variation of the input linear polarization angle.

Here, the reflection curve shows a distinct morphing behavior as a function of the polarization angle. For $\alpha = 45^\circ$, the two reflection dips merge into a single one at 8.76 THz. Here, the reflection dips to zero, which implies that a perfect absorber can be obtained at this frequency by rotating the input linear polarization rather than modifying the construction values of the metallic rods. Also, the reflection curve exhibits a smooth transition in the $7-8.5$ THz band, with values rising from 0.6 to 0.7, and then falling to 0.25 For $\alpha = 90^\circ$, the whole frequency-selective response collapses, and a fully-reflective metasurface is obtained. This implies that the metasurface cell can be used as a polarization-based dichroic mirror, especially at the resonance frequency, where a complete reflective-absorptive metasurface can be obtained by switching between $45^\circ$ and $90^\circ$ polarization states.

## 4. **Conclusions**

In this paper, we have performed investigations on the frequency-selective response of a metal-dielectric metasurface in the $7-10$ THz frequency band. We have chosen a ”T”-shaped metallic nanoantenna constructed out of two gold rods, deposited on a polyamide substrate. Under specific

variations of certain parameters of the configuration, the response in reflection changes from a fully-reflective to a fully-absorptive one. This behavior makes our configuration a viable candidate for obtaining polarization-based dichroic mirrors and attenuators, which represent a basis for many applications in this spectral window. When not at resonance, the metasurface exhibits a smooth spectral transition, indicating there are no parasitic surface oscillation modes on the interface, which renders our configuration ideal for dichroic broadband mirrors and attenuators.

**Acknowledgements**

We thank O. Dănilă for relevant discussions on metasurface simulation techniques and for corrections on the manuscript.

## REFERENCES

[1] N. Yu, P. Genevet, M. A. Kats, F. Aieta, J. P. Tetienne, F. Capasso, and Z. Gaburro. Light propagation with phase discontinuities: generalized laws of reflection and refraction. *Science*, 334(6054), 2011.

[2] O. Dănilă and D. Mănăilă-Maximean. Bifunctional metamaterials using spatial phase gradient architectures: generalized reflection and refraction considerations. *Materials*, 14(9), 2021.

[3] U. Leonhardt. Optical conformal mapping. *Science*, 312(5781), 2006.

[4] E. Arbabi, A. Arbabi, S. M. Kamali, Y. Horie, and A. Faraon. Controlling the sign of chromatic dispersion in diffractive optics with dielectric metasurfaces. *Optica*, 4(6):625–632, 2017.

[5] V. G. Veselago. The electrodynamics of substances with simultaneously negative values of $\varepsilon$ and $\mu$. *Soviet Physics Uspekhi*, 10(509), 1968.

[6] J. B. Pendry, A. J. Holden, D. J. Robbins, and W. J. Stewart. Magnetism from conductors and enhanced nonlinear phenomena. *IEEE Transactions on Microwave Theory and Techniques*, 47(11), 1999.

[7] W. Cai, U. K. Chettiar, A. V. Kildishev, and V. M. Shalaev. Optical cloaking with metamaterials. *Nature Photonics*, 1:224–227, 2007.

[8] D. Mănăilă-Maximean, C. Cîrtoaje, O. Dănilă, and D. Donescu. Novel colloidal system: magnetite-polymer particles/lyotropic liquid crystal under magnetic field. *Journal of magnetism and magnetic materials*, 438:132–137, 2017.

[9] D. Mănăilă-Maximean. Effective permittivity of a multiphase system: nanoparticle-doped polymer-dispersed liquid crystal films. *Molecules*, 26(5):1441, 2021.

[10] D. Mănăilă-Maximean, V. Cîrcu, P. Ganea, A. Bărar, O. Dănilă, T. Staicu, V. A. Loiko, A. V. Konkolovich, and A. A. Miskevich. Polymer dispersed liquid crystal films doped with carbon nanoparticles: electric and electro-optical properties. In *Advanced Topics in Optoelectronics, Microelectronics and Nanotechnologies X*, volume 11718, pages 117–182, 2020.

[11] B. A. Munk. *Frequency selective surfaces: theory and design*. Wiley and Sons Inc., 2005.

[12] D. R. Smith, W. J. Padilla, D. C. Vier, S. C. Nemat-Nasser, and S. Schultz. Composite medium with simultaneously negative permeability and permittivity. *Physical Review Letters*, 84(18), 2000.

[13] D. R. Smith, J. B. Pendry, and M. C. K. Wiltshire. Metamaterials and negative refractive index. *Science*, 305(5685), 2004.

[14] O. Dănilă. Spectroscopic assessment of a simple hybrid Si-Au metasurface-based sensor in the mid-infrared domain. *Journal of Quantitative Spectroscopy and Radiative Transfer*, 254(107209), 2020.

[15] O. Dănilă, D. Mănăilă-Maximean, A. Bărar, and V. A. Loiko. Non-layered gold-silicon and all-silicon frequency-selective metasurfaces for potential mid-infrared sensing applications. *Sensors*, 21(16), 2021.

[16] V. A. Loiko, A. V. Konkolovich, A. A. Miskevich, D. Mănăilă-Maximean, O. Dănilă, V. Cîrcu, and A. Bărar. Optical model to describe coherent transmittance of polymer dispersed liquid crystal film doped with carbon nanotubes. *Journal of Quantitative Spectroscopy and Radiative Transfer*, 245(106892), 2020.

[17] A. Bărar, O. Dănilă, D. Mănăilă-Maximean, and V. A. Loiko. Active spectral absorption control in a tunable liquid crystal/metamaterial structure by polarization plane rotation. In *International Conference on Nanotechnologies and Biomedical engineeering, Springer, Cham.*, pages 299–303, 2019.

[18] O. Dănilă. Polyvinylidene fluoride-based metasurface for high-quality active switching and spectrum shaping in the terahertz G-band. *Polymers*, 13(11), 2021.

[19] M. V. Gorkunov, M. V. Lapine, and S. A. Tretyakov. Methods of crystal optics for studying electromagnetic phenomena in metamaterials: review. *Crystallography Rep.*, 51:1048–1062, 2006.

[20] D. Schurig, J. J. Mock, B. J. Justice, S. A. Cummer, J. B. Pendry, A. F. Starr, and D. R. Smith. Metamaterial electromagnetic cloak at microwave frequencies. *Science*, 314(5801), 2006.

[21] J. B. Pendry. Negative refraction makes a perfect lens. *Physical Review Letters*, 85(3966), 2000.

[22] D. Arslan, K. E. Chong, A. E. Miroshnichenko, D. Y. Choy, D. N. Neshev, T. Pertsch, Kivsharm Y. S., and I. Staude. Angle-selective all-dielectric Huygens' metasurfaces. *J. Appl. Phys. D*, 50(434002), 2017.

[23] K. Koshelev, Y. Tang, K. Li, D. Y. Choi, G. Li, and Y. Kishvar. Nonlinear metasurfaces governed by bound states in the continuum. *ACS Photon.*, 6(7):1639–1644, 2019.